



## Synthesis of $g\text{-C}_3\text{N}_4$ -based photocatalysts with recyclable feature for efficient 2,4-dichlorophenol degradation and mechanisms

Mingna Chu, Kang Hu, Jinshuang Wang, Yanduo Liu, Sharafat Ali, Chuanli Qin\*, Liqiang Jing\*

Key Laboratory of Functional Inorganic Material Chemistry (Heilongjiang University), Ministry of Education, School of Chemistry and Materials Science, International Joint Research Center for Catalytic Technology, Harbin, 150080, PR China



### ARTICLE INFO

**Keywords:**

ACF-supported  $g\text{-C}_3\text{N}_4$   
Nickel-regulated carbon layer  
Phosphoric acid modification  
Charge transfer and separation  
Photocatalytic pollutant degradation

### ABSTRACT

It is highly desired to produce more  $\cdot\text{O}_2^-$  by regulating photogenerated electrons for efficiently degrading organic pollutants with recyclable feature. In this work,  $g\text{-C}_3\text{N}_4$ /active carbon fiber (ACF) photocatalysts with high activities for degrading 2,4-dichlorophenol (2,4-DCP) and bisphenol A (BPA) have been successfully fabricated via an *in-situ* thermal polycondensation method, attributed to the enhanced charge separation and promoted reactant adsorption from ACF. Moreover, the photocatalytic activities of optimized  $g\text{-C}_3\text{N}_4$ /ACF photocatalyst could be improved by introducing the carbon layer between them, especially for the nickel-regulated one. It is attributed to the promoted charge transfer and separation by improving the interface contacts between  $g\text{-C}_3\text{N}_4$  and ACF, and the function of introduced Ni species to  $\text{O}_2$  activation, mainly based on the fluorescence spectra related to the formed hydroxyl radical amounts, and the electrochemical oxygen reduction. Furthermore, the photocatalytic activities could be further improved by modifying phosphoric acid to promote the capture of photogenerated electrons by the increased adsorbed oxygen based on the  $\text{O}_2$  temperature-programmed desorption curves. Interestingly, it is shown that the optimal photocatalyst exhibits 10-time higher photocatalytic activities for 2,4-DCP degradation compared to bare  $g\text{-C}_3\text{N}_4$ . It is demonstrated through the radical-trapping experiments that  $\cdot\text{O}_2^-$  is the dominant active species to induce the degradation of 2,4-DCP, along with a suggested decomposition pathway according to the detected main intermediates. This further verifies this point that the photocatalytic activities for degrading organic pollutants could be efficiently improved by mediating electrons. As for the ACF-supported photocatalysts, a specific device has been designed to efficiently purify polluted water with convenient and continuous features. This work opens up a feasible route to develop a high-efficiency photocatalytic technology for recyclable degradation of environmental contaminants.

### 1. Introduction

The increasingly serious environmental pollution, especially water contamination has broken the balance of the natural ecosystem and endangered human health in recent years [1,2]. Therefore, the effective treatment of sewage is so necessary. The chlorophenols as the highly toxic organic pollutants are widely applied in pesticides, bactericides, insecticides, herbicides and wood preservatives [3,4]. Chlorophenols are difficult to biodegrade due to the high stability and have been listed by the U.S. Environment Protection Agency as a type of pollutant with priority control [5]. In particular, 2,4-DCP, a typical chlorophenol, is urgent to be removed from polluted water bodies because of its high stability and carcinogenicity [6–8]. Traditionally biological and electrocatalytic techniques have widely been explored. However, these techniques are always involved with less stability, catalyst poisoning,

and electrode corrosion [9–11]. Therefore, it is much meaningful to develop alternative techniques to overcome the above-mentioned shortfalls.

Nevertheless, semiconductor photocatalysis, as a ‘green’ chemistry technology using sunlight, has been attracting tremendous attention [12]. Photocatalysis can completely decompose organic pollutants even at low levels in an ambient environment [13]. In this regard, numerous semiconductor oxides, especially  $\text{TiO}_2$ , have been widely investigated. However, the ineffective utilization of solar light (only ca. 4% UV-light) and low quantum efficiency still greatly impair their applications [14–19]. Based on the large proportion of visible-light (ca. 46%) in the solar spectrum, it is highly desired to develop efficient narrow-bandgap photocatalysts to utilize visible-light. In recent years, the polymeric graphitic carbon nitride ( $g\text{-C}_3\text{N}_4$ , CN) with a narrow bandgap energy (2.7 eV) has attracted tremendous attention owing to its potential

\* Corresponding authors.

E-mail addresses: [qinchuanli@hlju.edu.cn](mailto:qinchuanli@hlju.edu.cn) (C. Qin), [jinglq@hlju.edu.cn](mailto:jinglq@hlju.edu.cn) (L. Jing).

applications in photocatalysis, superconductors, electrocatalysis and chemical sensors, etc. [20–22]. Its proper positions of valence band (VB) and conduction band (CB) are suitable for water splitting, CO<sub>2</sub> reduction and pollutant degradation [23–25]. Besides, due to its cheapness, high chemical and thermal stability, it can satisfy basic requirements for photocatalysis as a potential candidate for pollutant degradation [26]. Nevertheless, non-recyclability and low photocatalytic performance still limit its practical applications in environmental remediation. Thus, it is highly desired to develop a high-efficiency photocatalytic technology for the degradation of environmental pollutants on g-C<sub>3</sub>N<sub>4</sub>-based nanomaterials.

As for the purpose of effective recyclable utilization for nano-photocatalysts in practical applications, much effort has been made to select the suitable substrate in order to construct the supported photocatalysts. In general, the photocatalysts are often supported on glasses or metal foils [27]. These film-shaped photocatalysts can be efficiently recycled, but they still have some limitations like poor photocatalytic activities and high production cost. Another kind is free-standing semiconductor films as efficient and easily recyclable photocatalysts [28]. However, the mechanical properties of the free-standing film are unsatisfactory. Active carbon (AC) is widely used as a substrate in gas and water remediation because of its good adsorption for reactants [29]. However, AC is commonly used in the forms of granules and powders, and there remain some difficulties in recycling. While active carbon fiber (ACF) has attracted comprehensive attention as a carbon-based substrate with excellent flexibility and conductivity, high strength, low-cost and good recyclability in recent years [30]. At the same time, developing in-situ synthesis technology with ACF as the substrate is expected to facilitate the interface contact resulting in good charge transfer. Thus, it is much meaningful to obtain the recyclable photocatalyst with high activity by supporting CN onto ACF, however there are few related reports.

Unfortunately, the interface contacts between CN and ACF may not be satisfactory due to the smooth surface of ACF caused by high-temperature treatment. It is necessary to further improve the interface contacts between CN and ACF in order to promote charge transfer and separation. It is highly expected that the interfacial contacts between CN and ACF would be improved so that the charge transfer and separation would be facilitated by introducing a layer, which is carbon-based material as same as ACF. Moreover, thanks to the carbon layer with a disordered structure and defects formed in the process of crystal formation, the carbon layer would be introduced readily and effectively between CN and ACF [31]. In addition, the crystallization degree of the interfacial carbon layer is very important for charge transfer. The transition metals, like Fe, Co, Ni, etc., are expected to regulate the crystallization degree of the carbon layer [32,33]. At the same time, it is crucial to the oxygen activation during the photocatalytic pollutant degradation. Precisely, these transition metals, especially Ni, have the function of oxygen activation. Thus, it is expected to improve the photocatalytic activities of the supported photocatalysts through introducing transition metal-regulated carbon layer, especially for the nickel-regulated one. However, related works are rarely reported.

Generally, the reaction of photogenerated electrons with adsorbed oxygen is slow in the process of photocatalytic pollutant degradation, which is a key control step. Therefore, promoting O<sub>2</sub> adsorption is one of the important strategies to improve photocatalytic performance [34]. Surface modification is one of the effective methods to improve oxygen adsorption, thus obviously influencing the photocatalytic performance [35]. Based on the previous works in our group, it is an effective strategy that the surface modification is performed by phosphoric acid [36]. In addition, the 'O<sub>2</sub>' formed by the reaction of electrons and oxygen is very important in the reaction process, and it can effectively induce the degradation of 2,4-DCP. However, this degradation mechanism needs to be further confirmed. Therefore, it is of great significance to carry out phosphoric acid modification and further confirm the degradation mechanism of organic pollutants on the generated

'O<sub>2</sub>' through electronic regulation to induce the degradation. Besides, for the g-C<sub>3</sub>N<sub>4</sub>-based supported photocatalysts, a feasible reaction device for efficient and recyclable degradation of pollutants in industrial wastewater and contaminated drinking water is much needed.

Herein, we have successfully prepared the g-C<sub>3</sub>N<sub>4</sub>-based photocatalysts supported on ACF as an efficient photocatalyst for 2,4-DCP degradation through an in-situ thermal polycondensation method. The nickel-regulated carbon layer is introduced between CN and ACF to facilitate the photogenerated charge transfer and separation. Additional phosphoric acid is modified to promote O<sub>2</sub> adsorption so as to enhance the charge separation. Interestingly, the optimal supported photocatalysts exhibit significantly improved activities for 2,4-DCP degradation compared to bare CN, along with superior stability and recyclability. Moreover, it is confirmed that the photogenerated 'O<sub>2</sub>' could dominate the photocatalytic decomposition of 2,4-DCP, and it is much feasible to modulate the photogenerated electrons for the production of 'O<sub>2</sub>'. This work will provide a novel and effective route to design and prepare g-C<sub>3</sub>N<sub>4</sub>-based supported photocatalysts with high photocatalytic activities through a strategy of electronic regulation for recyclable purification of chlorophenol-polluted water environments.

## 2. Experimental

All the reagents were of analytical grade and used as received without further purification. Deionized water was used throughout the experiments.

### 2.1. Materials synthesis

#### 2.1.1. Synthesis of CN

CN was synthesized by heating melamine in 50 mL ceramic crucible at 570 °C for 3 h with the rate of 0.5 °C/min and after that, being cooled to the room temperature naturally. The obtained light-yellow product was grinded into fine powders for further experimental work.

#### 2.1.2. Pretreatment of active carbon fiber

ACF was purchased from Jinglong Special Carbon Company from Beijing, and cut into a circular shape with a diameter of 3 cm (the mass is about 0.2 g) by using a hole puncher. The pretreatment of ACF was carried out by immersing it in 2 M HNO<sub>3</sub> at 80 °C to remove the impurities, then followed by water washing and drying. The dried ACF was transferred to a tube furnace and heated in a nitrogen atmosphere at 400 °C for 2 h.

#### 2.1.3. Preparation of CN/ACF

The pretreated ACF was placed horizontally in 50 mL ceramic crucibles and completely covered with 6 g melamine, then heated in ceramic crucible at 570 °C for 3 h with the rate of 0.5 °C/min and after that, being cooled to room temperature naturally. The product was obtained for further experimental work. The samples were denoted as CN-ACF550, CN-ACF570, CN-ACF590, in which the number corresponds to the calcination temperature. The loading mass of CN is approximately 0.8 g on each sample.

#### 2.1.4. Preparation of CN/carbon layer-ACF

To obtain different CN/carbon layer-ACF samples, carbon layer-modified ACF was prepared as the substrate firstly. For this, different amounts of glucose (i.e. 0.5 g, 1 g, and 2 g) were dissolved in 50 mL deionized water. Then the cut ACF was fixed with gasket in the solution, transferred into a Teflon-lined autoclave and heated in an oven at 160 °C for 12 h. After being cooled to room temperature naturally, the obtained product was dried overnight at 60 °C in an oven and finally calcined in N<sub>2</sub> atmosphere at different temperatures (i.e. 500 °C, 600 °C, 650 °C) in a tubular furnace. Then, the synthetic processes similar to CN/ACF were carried out to prepare CN/carbon layer-ACF. The obtained samples were represented by CN/YCX-ACF, where 'X' stands for

the calcination temperature and 'Y' represents the mass of added glucose.

#### 2.1.5. Preparation of CN/nickel-regulated carbon layer-ACF

To obtain different CN/nickel-regulated carbon layer-ACF samples, different amounts of nickel nitrate were dissolved in 50 mL deionized water which contains a certain amount of glucose. Similarly, CN/(ZNi) YCX-ACF samples were obtained, where 'Z' represents the mass percentage of added nickel. As for CN/iron-regulated carbon layer-ACF and CN/cobalt-regulated carbon layer-ACF samples, the synthetic processes similar to CN/nickel-regulated carbon layer-ACF were carried out by replacing nickel nitrate with iron nitrate or cobalt nitrate.

#### 2.1.6. Preparation of phosphoric acid-modified CN/nickel-regulated carbon layer-ACF

To modify with different amounts of phosphoric acid to CN/(ZNi) YCX-ACF, the obtained CN/(ZNi)YCX-ACF was added into a certain concentration of phosphoric acid solution in a glass container under stirring for 1 h. Subsequently, it was dried at 80 °C for 24 h in an oven. The obtained samples were denoted as RP/CN/(ZNi)YCX-ACF, in which 'R' is the mass percentage of used phosphoric acid to CN, and 'P' represents phosphoric acid.

### 2.2. Characterization techniques

The samples were analyzed by various techniques. The X-ray diffraction (XRD) was tested with a Rigaku D/MAX-rA powder diffractometer, using Cu K $\alpha$  radiation. The UV-vis diffuse reflectance spectra (DRS) of the samples were measured with a Model Shimadzu UV2550 spectrophotometer, using BaSO<sub>4</sub> as a reference. The Fourier-transform infrared (FT-IR) spectra of the samples were collected with a Bruker Equinox 55 spectrometer, using KBr as diluents. Scanning electron microscopy (SEM) images were taken using a Hitachi S-4800 instrument, operated at acceleration voltage of 15 kV. Raman spectra were performed with a Jobin Yvon HR 800 micro-Raman spectrometer at 457.9 nm. The laser beam was focused with a 50  $\times$  objective lens to a ca. 1  $\mu$ m spot on the surface of the sample. The photoluminescence (PL) spectra of the samples were measured with a spectrofluoro-photometer (LS55 Perkin-Elmer) at excitation wavelength of 390 nm. The X-ray photoelectron spectroscopy (XPS) was examined by using a Kratos-Axis Ultra DLD apparatus equipped with an Al (mono) X-ray source, and the binding energies were calibrated with respect to the signal for adventitious carbon (binding energy = 284.6 eV).

#### 2.3. Measurement for O<sub>2</sub> temperature-programmed desorption curves

The temperature-programmed desorption (TPD) curves of O<sub>2</sub> were measured with a home-built flow apparatus. The typical method is as follows. 50 mg of sample was pretreated at 270 °C for 0.5 h with an ultra-high-purity Helium (He) flow. After that, the system was cooled to room temperature and then the sample was blown continuously with O<sub>2</sub> for 90 min at 30 °C. Subsequently, He was passed through the system to remove O<sub>2</sub>. Finally, the O<sub>2</sub>-TPD profiles of the sample were recorded by increasing the temperature from 30 to 550 °C at a heating rate of 10 °C/min under the He flow. The desorbed O<sub>2</sub> was analyzed by a gas chromatograph (GC-2014, Shimadzu) with a TCD detector.

#### 2.4. Photoelectrochemical (PEC) measurements

The PEC experiments were performed in a three-electrode cell with a Platinum plate (99.9%) as the counter electrode, and a saturated KCl Ag/AgCl electrode (SSE) as the reference electrode on a LK2006 A workstation. The working electrode (the illumination area is about 1 cm<sup>2</sup>) was positioned in 1 M Na<sub>2</sub>SO<sub>4</sub> electrolyte with the obtained sample. High purity O<sub>2</sub> was used to bubble through the electrolyte before and during the electrochemical O<sub>2</sub> reduction experiments.

Electrochemical impedance spectra (EIS) were measured using the same three-electrode configuration with the Princeton Applied Research Versa STAT 3 and carried out over the frequency range from 10<sup>2</sup> to 10<sup>5</sup> Hz with amplitude of 10 mV (RMS) in a 1 M Na<sub>2</sub>SO<sub>4</sub> solution. The electrodes were illuminated with a 150 W Xenon lamp.

#### 2.5. Evaluation of produced hydroxyl radical (·OH) amounts and photocatalytic activities

As for the ACF-supported photocatalysts, a specific device has been designed by ourselves to evaluate the produced ·OH amounts and photocatalytic activities (as shown in Fig. S1), which is suitable for the efficient and recyclable treatment of organic wastewater.

To measure the ·OH amounts, the supported photocatalyst was placed in our own designed device, then 50 mL of 1  $\times$  10<sup>-3</sup> mol/L coumarin aqueous solution was added into a quartz reactor and magnetically stirred for 10 min to reach adsorption-desorption equilibrium. Each sample was irradiated for 60 min under 150 W Xenon lamp. After centrifugation, a certain amount of the solution was taken in a Pyrex glass cell for fluorescence measurement of 7-hydroxycoumarin at 390 nm excitation wavelength and 460 nm emission wavelength through a spectrofluorometer (Perkin-Elmer LS55).

The photocatalytic activities of the samples were evaluated by the degradation of 2,4-DCP. For 2,4-DCP degradation, the supported sample and 100 mL of 80 mg/L 2,4-DCP solution were added into our own designed device under magnetic stirring at room temperature and standard pressure. Before irradiation, the mixture was stirred magnetically in dark for 60 min to reach adsorption-desorption equilibrium. After irradiation for certain time, the solution was centrifuged and then its 2,4-DCP concentration was measured with a Shimadzu UV-2550 spectrophotometer through the 4-aminoantipyrine spectrophotometric method at the characteristic optical absorption. In addition, for the photocatalytic degradation of bisphenol A (BPA), the supported sample and 100 mL of 80 mg/L BPA solution were used, and the experiments were performed in a similar way to the photocatalytic degradation of 2,4-DCP.

#### 2.6. Measurements of produced intermediates

The intermediates were detected during the photocatalytic degradation of 2,4-DCP. In a typical experiment, the supported sample and 100 mL of 80 mg/L 2,4-DCP solution were added into our own designed device under magnetic stirring at room temperature and standard pressure for 60 min in the dark to maintain the adsorption-desorption equilibrium of the reaction system. After that, the system began to be irradiated with 150 W Xenon lamp for 3 h. At the interval of every 0.5 h, a planned amount of the solution was centrifuged and the concentration of 2,4-DCP was analyzed by UV spectrometer. The intermediates were analyzed with Agilent liquid chromatography tandem mass spectrometry (LC/MS, 6410MS) technique. The intermediate fragments of the main reaction were analyzed through scan mode.

### 3. Results and discussion

#### 3.1. Effects of ACF as the substrate on CN

The SEM micrographs of ACF and CN/ACF570 are shown in Fig. S2A and B, respectively. As shown in Fig. S2A, the surface of ACF is almost clean and smooth, the fibers with a diameter of ~10  $\mu$ m are weaved together in a sheet. In comparison, it can be found from Fig. S2B that the CN/ACF570 presents a rough surface suggesting the successful adhesion of CN to ACF. The crystal composition and structure of the synthesized samples were analyzed by XRD patterns. In Fig. S2C, the XRD patterns of CN show two characteristic diffraction peaks at 20 of 13.1° and 27.3°, respectively, corresponding to the (100) and (002) reflections of CN [24]. Compare to pure CN, the CN/ACF570 shows an

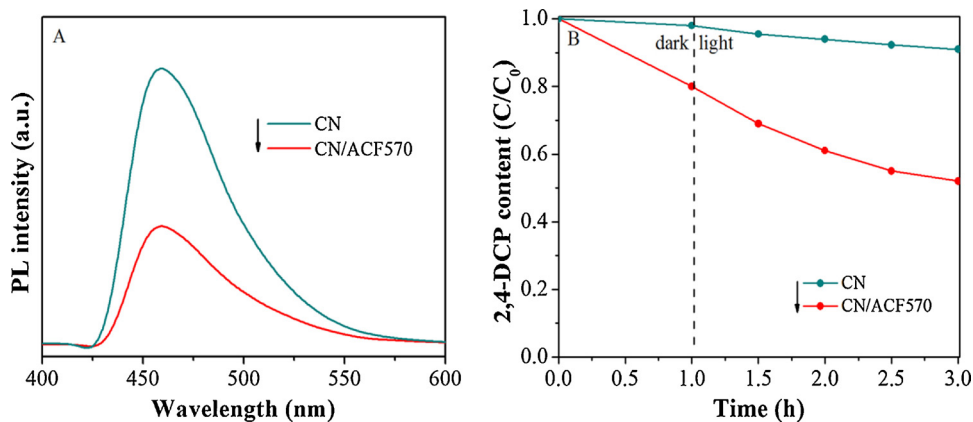


**Fig. 1.** PL spectra (A) and photocatalytic 2,4-DCP degradation activities (B) of CN and CN/ACF570. (In the description below, CN/ACF570 is abbreviated as CN/ACF.)

additional peak at 2θ of 22.0°, identified as the (002) plane of the carbon structure of ACF, which strongly supports the successful loading of CN on the surface of ACF. Besides, no impurity peaks can be observed except for CN and ACF. DRS were measured as shown in Fig. S2D and it is clear that CN displays strong reflection band edge at about 470 nm which corresponds to the intrinsic band gap of approximately 2.7 eV, which is calculated by a widely accepted equation,  $Eg = 1240/\lambda$  [37,38]. And the ACF as the substrate does not affect the band edge, with only a little effect on the light absorption in visible region. These results clearly demonstrate that the CN has been successfully supported on ACF.

The separation of photoexcited charges was studied by PL measurement at 390 nm excitation wavelength as shown in Fig. 1A. It is widely accepted that PL intensity is directly related to the recombination of electron-hole pairs. It is observed that CN shows an intense and broad emission peak centered at about 470 nm due to band-band transition, indicating high charge recombination rate in CN. Noticeably, the PL signal of CN/ACF570 is significantly decreased, due to the fact that the ACF can accept and transfer photoelectrons to hinder the recombination process, resulting in the enhanced charge separation. Is it possible to verify the enhanced charge separation by the crucial photochemical radical product, ·OH? For this, the FS spectra related to the produced ·OH amounts are shown in Fig. S2E, in which the coumarin could easily react with formed ·OH and produce luminescent 7-hydroxy-coumarin. As demonstrated earlier, the ·OH amounts could effectively reveal the separation of photogenerated charges in the photocatalysis. It is clearly seen that pure CN produces a small amount of ·OH, and after supporting with ACF, the amount of produced ·OH obviously increases. Obviously, it is in good agreement with the above PL results. Therefore, it could be concluded that the photogenerated charge separation of CN is enhanced by introducing ACF as a substrate. It also indicates that there will be good photocatalytic activities. Fig. 1B displays the photocatalytic activities of different samples for 2,4-DCP degradation. It is clearly seen that pure CN exhibits poor photocatalytic activities for 2,4-DCP degradation. After supporting with ACF, the adsorption rate can reach about 20%, indicating that ACF has the high adsorption capability for reactants, and the photocatalytic activities of CN for 2,4-DCP degradation have been greatly improved. It is in agreement with the above PL and FS results. Therefore, it is concluded that the improved photocatalytic activities are mainly attributed to the high adsorption capability of ACF for reactants, and the enhanced photogenerated charge transfer and separation due to the ACF as a good electron transporter.

In the process of synthesizing supported samples by the developed in-situ thermal polymerization, the calcination temperature is critical, so we explored the optimal calcination condition. Based on XRD patterns and DRS spectra shown in Fig. S3A and B, it is seen that the phase

composition and band gap of the samples prepared at different calcination temperatures remain unchanged. As shown in Fig. S3C and D, the optimized CN/ACF570 shows the lowest PL intensity, the highest produced ·OH amounts and the highest photocatalytic activities, probably because CN prepared at 570 °C has the optimal electronic structure and specific surface area. Therefore, it is concluded that the optimal calcination temperature is 570 °C, and in the description below, CN/ACF570 is abbreviated as CN/ACF.

### 3.2. Effects of introduced carbon layer between CN and ACF on CN/ACF

The SEM image in Fig. S4A shows that the microstructure remains unchanged after introducing carbon layer. XRD patterns and DRS spectra in Fig. S4B and C show that the phase compositions and band edges also remain unchanged after introducing carbon layer. It is confirmed based on Fig. 2A that the amount of ·OH produced by CN/1CX-ACF is much higher than that by CN/ACF, especially for the calcination temperature-optimized CN/1C600-ACF, which displays the strongest FS intensity corresponding to the highest charge separation. As shown in Fig. S4D, the PL intensity of CN/1CX-ACF is significantly decreased after introducing carbon layer, and the CN/1C600-ACF exhibits the lowest PL response, indicating the lowest recombination of electron-hole pairs. It is consistent with the results of above FS spectra. As expected, the photocatalytic activities of samples are significantly improved after the introduction of carbon layers, especially for CN/1C600-ACF, as shown in Fig. 2B. In addition to the calcination temperature, we have also investigated the effect of the glucose amounts on photocatalytic activities. As expected, CN/1C600-ACF with the optimal amount of 1 g glucose exhibits the best activities according to Fig. S5. It is worthy of noting that the carbon layer introduced under appropriate conditions could make the interfaces between CN and ACF contact closely, leading to the enhanced charge separation so as to the improved photocatalytic activities.

### 3.3. Effects of regulated carbon layer by nickel on CN/ACF

It is necessary to increase the graphitization degree of carbon layer through regulating it with nickel. On the basis of XRD patterns in Fig. S6A, there is no new XRD peak after introducing the nickel-regulated carbon layer, and it is important to note that typical peaks of Ni species are not observed, possibly due to the tiny amounts of modifying Ni. And it can be seen from DRS spectra in Fig. S6B that band edges are also unchanged after regulating carbon layer by nickel. The surface functional groups and elemental states of CN/1C600-ACF and CN/(1Ni)1C600-ACF were characterized by XPS. The XPS spectra of C1s for the two samples (Fig. S6C) exhibit two peaks at binding energies of 284.6 eV and 288.3 eV, corresponding to C=C band and C—N—C band,

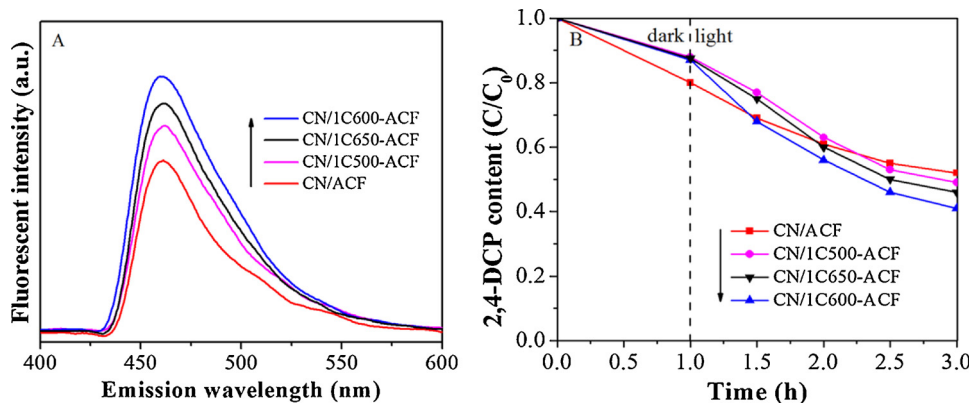


**Fig. 2.** FS spectra of the formed hydroxyl radicals (A) and photocatalytic 2,4-DCP degradation activities (B) of CN/ACF and CN/1CX-ACF, in which number 1 represents the mass of the added glucose (g) and 'X' stands for the calcination temperature.

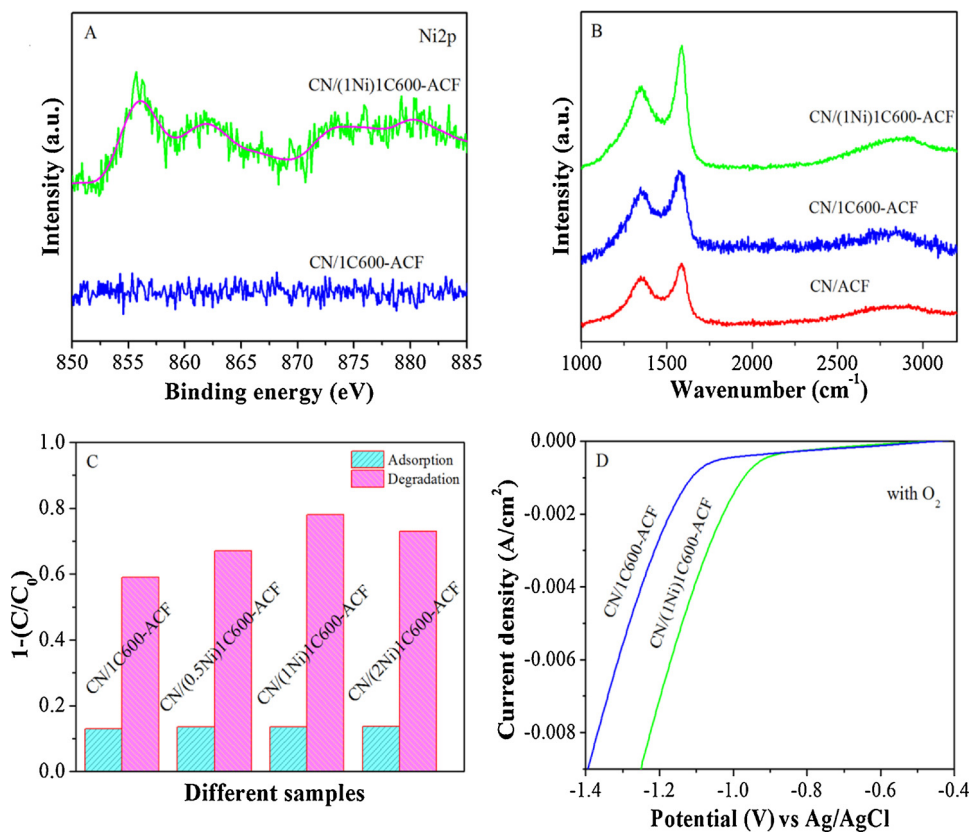


**Fig. 3.** XPS spectra of Ni2p (A), Raman spectra (B), photocatalytic 2,4-DCP degradation activities (C) and electrochemical reduction curves in the  $O_2$ -bubbled (D) of CN/1C600-ACF and CN/(ZNi)1C600-ACF, in which 'Z' stands for the mass percentage of nickel.

respectively. The XPS spectra of N1s for the two samples (Fig. S6D) show that the main N1s peak at 398.6 eV is attributed to  $sp^2$ -hybridized nitrogen ( $C=N-C$ ) and the weak characteristic peaks at 399.8 eV and 401.5 eV are assigned to the bond energies of N in  $N-(C)_3$  and  $C-N-H$ , respectively [39]. As shown in Fig. 3A, the XPS spectrum of Ni2p for CN/(1Ni)1C600-ACF exhibits the peaks centered at 851–865 and 870–885 eV with the main peaks and satellite peaks, attributed to the  $Ni^{2+}$  and  $Ni^{3+}$  spin-orbit levels of NiO [40]. In Fig. S6E, the O1s of CN/1C600-ACF shows only one peak at 531.8 eV, attributed to hydroxyl oxygen. But for CN/(1Ni)1C600-ACF, the extra peak locates at 529.3 eV, attributed to the possible formation of lattice oxygen [41,42]. These verify the existence of NiO in the regulated carbon layer. In order to determine the graphitization degree of the carbon layer, Fig. 3B gives the Raman patterns of CN/ACF, CN/1C600-ACF and CN/(1Ni)1C600-

ACF, which exhibit two peaks of "D-band" at  $\sim 1350\text{ cm}^{-1}$  and "G-band" at  $\sim 1560\text{ cm}^{-1}$ . The G band represents the characteristic peak of graphitic carbon and the D band represents the characteristic peak of amorphous carbon. The ratio of peak intensity ( $I_G/I_D$ ) reflects the graphitization degree of samples, and the larger the ratio, the higher the graphitization degree [43]. It can be seen that  $I_G/I_D$  has not changed significantly after introducing carbon layer between CN and ACF, but it obviously increases after introducing nickel-regulated carbon layer, indicating that the graphitization degree of carbon layer between CN and ACF could be greatly promoted through nickel regulation.

As expected, CN/(ZNi)1C600-ACF exhibits improved photocatalytic activities for 2,4-DCP degradation as shown in Fig. 3C and CN/(1Ni)1C600-ACF displays the highest activity with a 20% degradation rate enhancement compared with non-nickel-regulated one (CN/1C600-

ACF). It is in agreement with the corresponding amount of produced ·OH and PL intensity as shown in Fig. S6F. Thus, it is confirmed that the introduction of nickel-regulated carbon layer could promote charge separation, which is responsible for the improved photocatalytic activities. To further explore the enhanced charge separation mechanism after introducing nickel-regulated carbon layer, the electrochemical O<sub>2</sub> reduction of different samples was measured as shown in Fig. 3D. It is demonstrated that the activating oxygen of NiO is responsible for the enhanced reduction current of O<sub>2</sub> at the same applied voltage and decreased onset potential of O<sub>2</sub> reduction. Interestingly, the electrochemical O<sub>2</sub> reduction results are further supported by O<sub>2</sub>-TPD (Fig. S6G). The O<sub>2</sub>-TPD test is used to test the amount of adsorbed oxygen on samples. The stronger TPD signal implies the larger amount of adsorbed O<sub>2</sub>. [44,45]. In general, the desorptions at low and high (over 350 °C) temperature are attributed to the physically and chemically adsorbed forms, respectively. As shown in Fig. S6G, it is found that the amounts of desorbed O<sub>2</sub> for CN/1C600-ACF obviously increase after regulating the carbon layer with nickel, especially for the chemically desorbed O<sub>2</sub>. This shows that for the sample with the nickel-regulated carbon layer can adsorb much oxygen and then facilitate oxygen activation, so as to promote the photogenerated charge separation and then be favorable for photocatalytic reactions. This fully indicates that the photocatalytic activities of CN/1C600-ACF are greatly improved by regulating carbon layer with nickel.

In order to further confirm the function of NiO to activate oxygen, we designed a comparative experiment of washing NiO with 2 M HNO<sub>3</sub>. As shown in Fig. S7A, the sample washed with 2 M HNO<sub>3</sub> (noted as CN/(0Ni)1C600-ACF) has a lower ability to degrade 2,4-DCP than CN/(1Ni)1C600-ACF. The depressed photoactivities are attributed to the low photogenerated charge separation after washing out NiO based on the produced ·OH amounts and PL spectra as shown in Fig. S7B. What causes the charge separation to attenuate? As shown in Fig. S7C and D, after washing out nickel, there is almost no activation for oxygen, resulting in the reduced photocatalytic activities.

As described above, the graphitization degree of the carbon layer could be enhanced through the regulation by nickel, thereby promoting charge transport. In addition, nickel oxide could activate O<sub>2</sub> so as to enhance the charge separation and hence to improve the photocatalytic activities. To verify the effects of regulating carbon layer with other transition metals, we have also carried out the regulation of carbon layer by other two metals, namely iron and cobalt, with the same amount as that of the optimized nickel (1%). As shown in Fig. S8A and B, there are no new XRD peaks and the band edge of CN/1C600-ACF has not been changed after regulating carbon layer by iron and cobalt. Hence, it is concluded that the crystal phase composition and band gap of the regulated carbon layers by iron or cobalt do not change. To investigate whether iron or cobalt is modified on the carbon layer, XPS measurements were performed. In the high-resolution spectrum of Fe2p for CN/(1Fe)1C600-ACF (Fig. S8C), two intense peaks, observed at 711.3 eV with a shake-up satellite line at 719 eV and 724.4 eV, correspond to Fe<sup>3+</sup> in Fe<sub>2</sub>O<sub>3</sub>, and the lineshape and binding energies of Fe2p are agree well with the literature values for Fe<sub>2</sub>O<sub>3</sub> [46]. The XPS spectrum of Co2p exhibits two peaks at 795.6 eV and 780.2 eV, corresponding to the Co2p<sub>1/2</sub> and Co2p<sub>3/2</sub> spin-orbit peaks of Co<sub>3</sub>O<sub>4</sub> (Fig. S8D), respectively [47]. According to the XPS results, it is confirmed that the iron and cobalt are successfully introduced on the carbon layer. The Raman patterns of the four samples (Fig. S8E) confirm that the introduction of Fe- and Co-regulated carbon layer can also increase the graphitization degree of carbon layers, but the improvement degree does not reach that of Ni-regulated one.

To investigate the photocatalytic activities of CN/transition metal-regulated carbon layer-ACF, photocatalytic experiments for degrading 2,4-DCP have been carried out. As shown in Fig. 4A, the degradation rates of CN/transition metal-regulated carbon layer-ACF are obviously higher than that of CN/carbon layer-ACF. The degradation activities of CN/(1Co)1C600-ACF are higher than those of CN/(1Fe)1C600-ACF.

And the CN/(1Ni)1C600-ACF shows the highest degradation activity, with a approximately 20% enhancement than that of CN/1C600-ACF. Which is in agreement with the corresponding amount of produced ·OH and PL intensity as shown in Fig. S8F. To explore the enhanced charge separation mechanism after regulation of transition metals on carbon layer, we measured the electrochemical O<sub>2</sub> reduction of different samples. As shown in Fig. 4B, it is worthy of noting that all the samples regulated by iron, cobalt and nickel can activate oxygen, and the nickel-regulated sample has the most obvious effect. It is beneficial for capturing photogenerated electrons and promoting charge separation so as to improve photocatalytic activities.

### 3.4. Effects of phosphoric acid modification on CN/C-ACF

On the basis of XRD patterns (Fig. S9A) and DRS spectra (Fig. S9B), it is suggested that the phase compositions and band edges are unchanged after phosphoric acid modification. To investigate whether the phosphate groups are modified on the surface of CN/(1Ni)1C600-ACF, XPS measurements of 5P/CN/(1Ni)1C600-ACF and CN/(1Ni)1C600-ACF were performed. As illustrated in Fig. S9C and D, it can be seen that the C1s spectra of unmodified and phosphate modified ones are similar, and N1s spectra are also. The O1s spectra of both samples are shown in Fig. S9E. It can be seen that after phosphoric acid modification, the hydroxyl oxygen species decrease due to the fact that they are replaced by the [PO<sub>4</sub>]<sup>3-</sup> groups [36]. Whereas, the XPS peak of P2p at about 133.2 eV for 5P/CN/(1Ni)1C600-ACF (Fig. 5A) indicates that the phosphate groups have been modified on the surface of sample [48]. It is further confirmed by FT-IR spectra (Fig. S10A) that a new peak is observed at about 1090 cm<sup>-1</sup>, assigned to the characteristic of phosphate groups [49]. The above XPS and FT-IR results indicate that the phosphate groups have been successfully modified on the surface of CN/(1Ni)1C600-ACF.

As expected, the phosphoric acid-modified ones display enhanced photocatalytic activities for 2,4-DCP degradation, as shown in Fig. 5B, and 5P/CN/(1Ni)1C600-ACF with the optimal phosphoric acid amount shows the highest photoactivity with an approximately 14% enhancement compared to the non-phosphoric acid-modified one. This is further supported by the PL spectra and FS spectra related to the produced ·OH amounts (Fig. 5C). The O<sub>2</sub>-TPD analysis (Fig. 5D) and electrochemical O<sub>2</sub> reduction analysis (Fig. S10B) indicate that the O<sub>2</sub> adsorption of 5P/CN/(1Ni)1C600-ACF is obviously higher after modifying with an appropriate amount of phosphoric acid compared to CN/(1Ni)1C600-ACF. This would effectively facilitate the charge separation so as to improve photocatalytic activities for 2,4-DCP degradation.

### 3.5. Discussion on mechanism

The increased charge separation is also confirmed by the EIS measured under irradiation, as shown in Fig. 6 A. According to previous reports, the smaller arc radii always exhibits higher charge separation [50]. It is clear that the capacitive arc radius of 5P/CN/(1Ni)1C600-ACF is remarkably decreased, compared to those of CN/ACF, CN/1C600-ACF and CN/(1Ni)1C600-ACF. This indicates the charge recombination is significantly reduced, which is consistent with the previous photocatalytic activities.

To further confirm the improved photocatalytic activities, the photocatalytic activities of the as-prepared samples were evaluated for BPA degradation and the results are shown in Fig. 6B. Similarly, it is clear that the photocatalytic activities for BPA degradation are improved gradually through introducing carbon layer and then introducing nickel-regulated carbon layer between CN and ACF. Interestingly, it is noticed that after further modifying phosphoric acid with the optimal amount, the photocatalytic activities for BPA degradation are remarkably improved and the highest photoactivities are observed for 5P/CN/(1Ni)1C600-ACF.

In general, superoxide radicals (·O<sub>2</sub><sup>-</sup>), active holes (h<sup>+</sup>) or

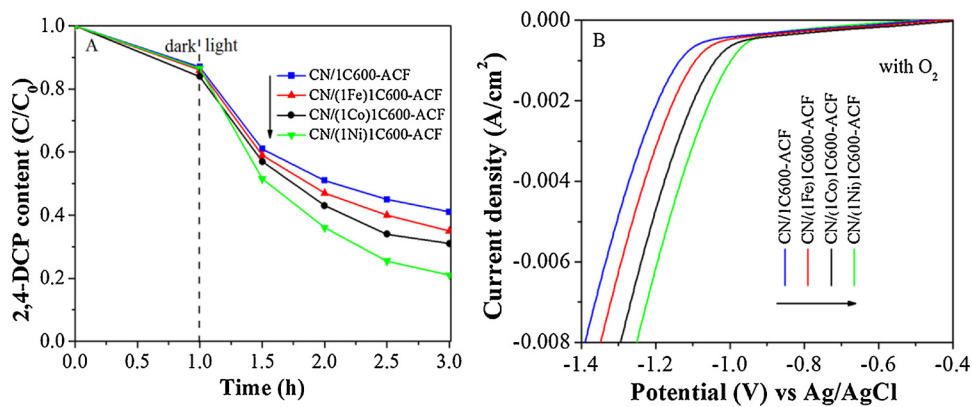


**Fig. 4.** Photocatalytic 2,4-DCP degradation activities (A) and electrochemical reduction curves in the O<sub>2</sub>-bubbled (B) of CN/1C600-ACF, CN/(1Fe)1C600-ACF, CN/(1Co)1C600-ACF, and CN/(1Ni)1C600-ACF.

hydroxyl radicals (·OH) participates in the reaction as the main attacking species during the photocatalytic degradation of organic pollutants. In order to further investigate the mechanism of 2,4-DCP degradation, ethylenediamine tetraacetic acid disodium salt (EDTA-2Na), benzoquinone (BQ) and isopropanol (IPA) are used as scavengers to study the effects of h<sup>+</sup>, ·O<sub>2</sub><sup>−</sup> and ·OH in the reaction. A series of experiments were carried out to examine the effects of different reactive species on the photodegradation rate of 2,4-DCP. As shown in Fig. 6C, with 1 mM of EDTA-2Na or IPA added to the system of 5P/CN/(1Ni) 1C600-ACF, there is no significant change in the degradation rate of 2,4-DCP compared to absence of any scavenger degradation. However, 1 mM of BQ added to the reaction system results in a significant decrease in degradation rate. Therefore, it can be deduced that ·O<sub>2</sub><sup>−</sup> is the vital species in the 2,4-DCP degradation by 5P/CN/(1Ni)1C600-ACF. Therefore, it is concluded that the improved photocatalytic activities of

CN/ACF after introducing a nickel-regulated carbon layer and further modifying phosphoric acid are mainly attributed to the regulation of electrons.

To further explain the degradation mechanism, the intermediates during the 2,4-DCP degradation by 5P/CN/(1Ni)1C600-ACF were analyzed by liquid chromatography tandem mass spectrometry. All the mass spectra of the intermediates are shown in Fig. S11A–C. According to the monitored intermediates, we hypothesize a reasonable pathway for the 2,4-DCP degradation by 5P/CN/(1Ni)1C600-ACF in Scheme 1. Based on the activity of ·OH on the aromatic ring of 2,4-DCP, the ortho- or para-position Cl<sup>−</sup> of 2,4-DCP is easily substituted by ·O<sub>2</sub><sup>−</sup> through an addition reaction. Accordingly, ·O<sub>2</sub><sup>−</sup> attack and removal of the ortho-position Cl<sup>−</sup> are proposed as the first step to form a para-chlorophenol super oxide radical (*m/z* = 159, Fig. S11 A in the Extract ion chromatography). The structure identification is further supported

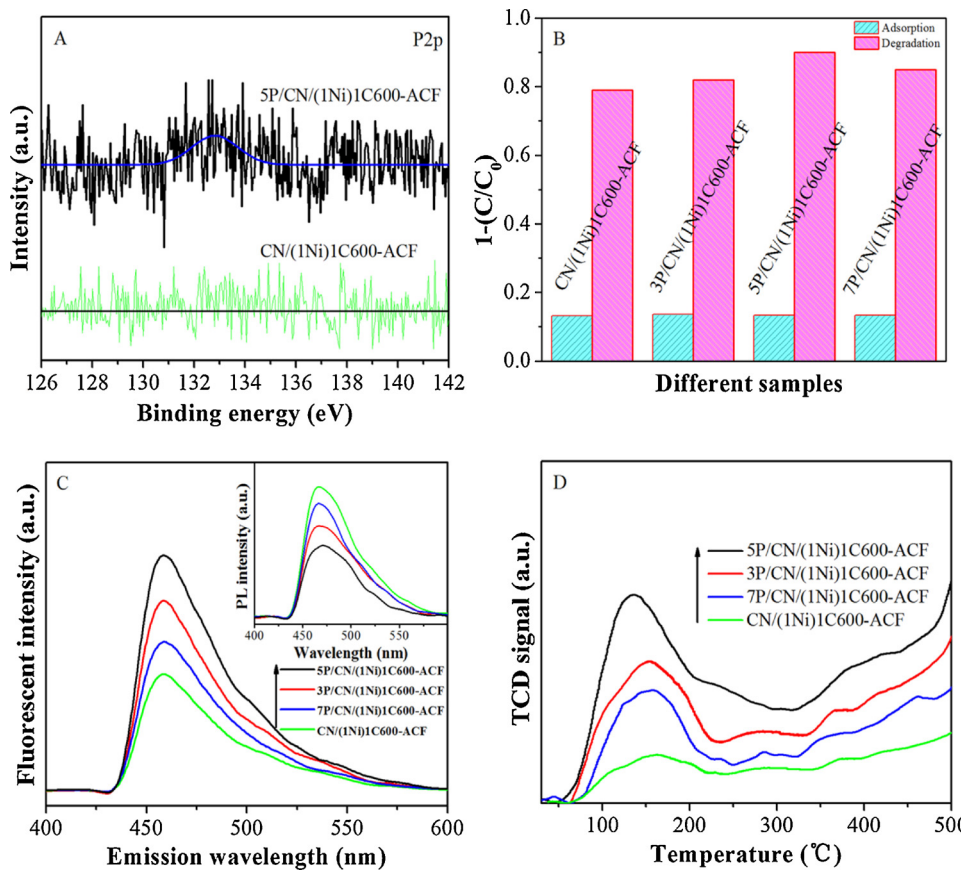


**Fig. 5.** XPS spectra of P2p (A), photocatalytic 2,4-DCP degradation activities (B), FS spectra of the formed hydroxyl radicals with inset PL spectra (C) and O<sub>2</sub>-TPD curves (D) of CN/(1Ni) 1C600-ACF and RP/CN/(1Ni)1C600-ACF, in which 'R' stands for the mass percentage of used phosphoric acid to CN/(ZNi)XCY-ACF, and 'P' stands for phosphoric acid.

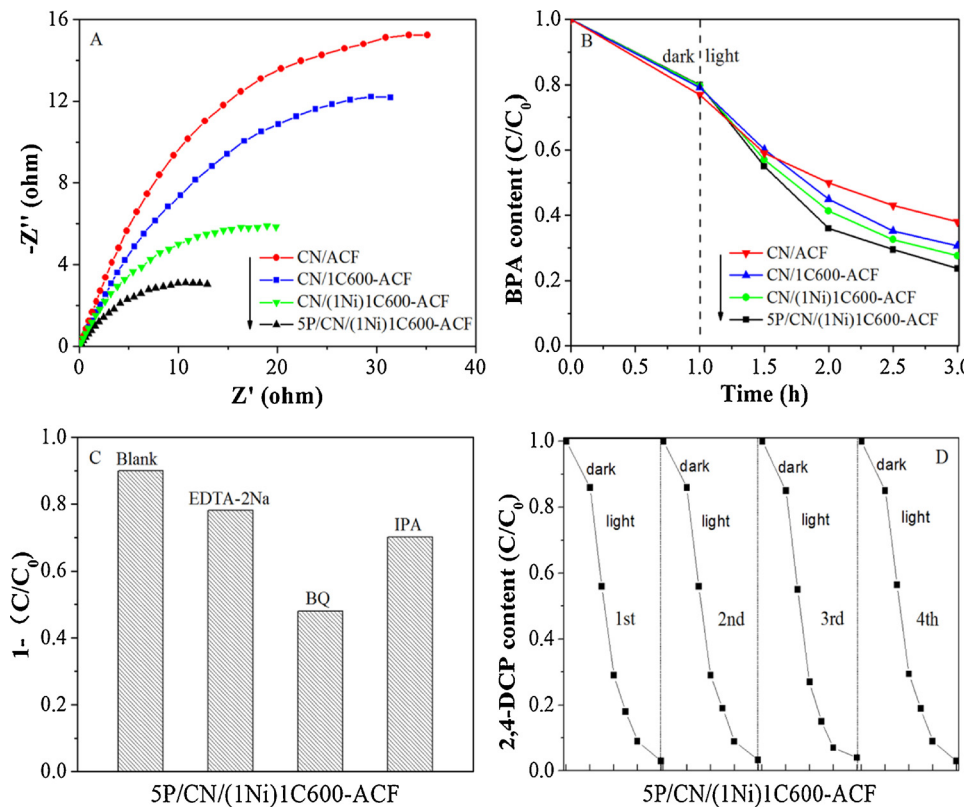
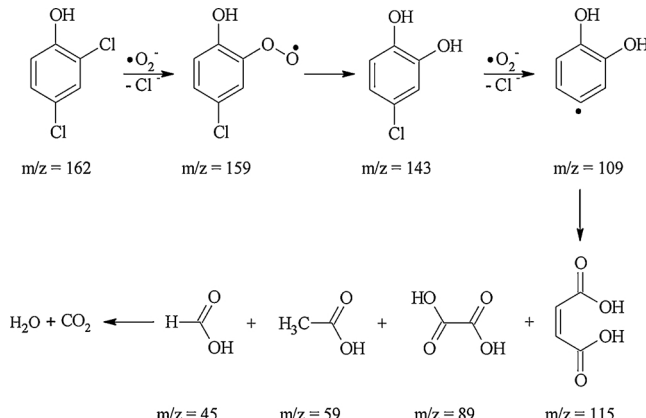


**Fig. 6.** Electrochemical impedance spectra (A), photocatalytic BPA degradation activities (B) of CN/ACF, CN/1C600-ACF, CN/(1Ni)1C600-ACF and 5P/CN/(1Ni)1C600-ACF, photocatalytic degradation rates of 2,4-DCP in the presence of IPA, BQ and EDTA-2Na after irradiation for 3 h (C) and the stability (D) of 5P/CN/(1Ni)1C600-ACF for 2,4-DCP degradation.



**Scheme 1.** Proposed pathway for 2,4-DCP degradation on 5P/CN/(1Ni)1C600-ACF.

by the LC-MS/MS data with product ion fragments inset in Fig. S11A in the EIC. 4-chlorocatechol ( $m/z = 143.5$ , Fig. S11B) is produced from the second step of the degradation pathway [51]. As for the process of removing the second  $Cl^-$ ,  $\cdot O_2^-$  would directly attack and then produce 2-hydroxyphenol ( $m/z = 109$ , Fig. S11C). Then the target product continues ring-opening cleavage to generate maleic acid ( $m/z = 115$ ), oxalic acid ( $m/z = 89$ ), acetic acid ( $m/z = 59$ ) and formic acid ( $m/z = 45$ ). Finally, these kinds of acids can be mineralized to  $CO_2$  and  $H_2O$  [52].

To further investigate the stability of 5P/CN/(1Ni)1C600-ACF, we measured its four consecutive cycles of degrading 2,4-DCP under irradiation (Fig. 6D). It is seen that no significant change is observed in the photocatalytic activities during four runs. And after four cycles, the weight of 5P/CN/(1Ni)1C600-ACF nearly remains unchanged. These facts demonstrate that 5P/CN/(1Ni)1C600-ACF has excellent stability and recyclability.

In order to further understand the photocatalytic activity

improvement of phosphoric acid-modified CN/nickel-regulated carbon layer-ACF, a mechanism schematic is proposed as shown in Fig. 7. ACF is able to adsorb reactants on its surface, while ACF acts as an electron transporter to promote charge separation and thus enhance photocatalytic activities. The introduction of nickel-regulated carbon layer between CN and ACF contributes to electron transport through the interfacial regulation, and at the same time, NiO can activate oxygen to promote the capture of photogenerated electrons. After a proper amount of phosphoric acid is modified on the surface of CN/(1Ni)1C600-ACF, the ability of adsorbing  $O_2$  is further greatly increased. Thus, these lead to the increased charge transfer and separation so as to improve photocatalytic activities for 2,4-DCP degradation. During the above reaction, the formed intermediate  $\cdot O_2^-$  as the product of electron modulation plays an important role in the degradation of pollutants. In particular, it is confirmed that the formed  $\cdot O_2^-$  effectively attacks 2,4-DCP to initiate the degradation.

#### 4. Conclusions

In summary, the CN/ACF supported photocatalyst with strong adsorption for reactants has been successfully fabricated via an in-situ thermal polycondensation method. Its photocatalytic activities for degrading 2,4-DCP have been greatly improved through firstly introducing nickel-regulated carbon layer between CN and ACF and subsequently modifying with phosphoric acid. It is shown that the optimal photocatalyst has exhibited more favorable photocatalytic performance, which is approximately ten-time enhancement for 2,4-DCP degradation compared to bare CN powder. As confirmed by PL, electrochemical oxygen reduction,  $O_2$ -TPD and EIS measurements, the superior photocatalytic activities are attributed to the facilitated charge transfer and separation due to the fact that the graphitization degree of carbon layer introduced between CN and ACF is increased through nickel regulation, and at the same time NiO could play a role of activating oxygen. Besides, the phosphoric acid modification could further promote the photogenerated electrons to adsorb  $O_2$ , resulting in the

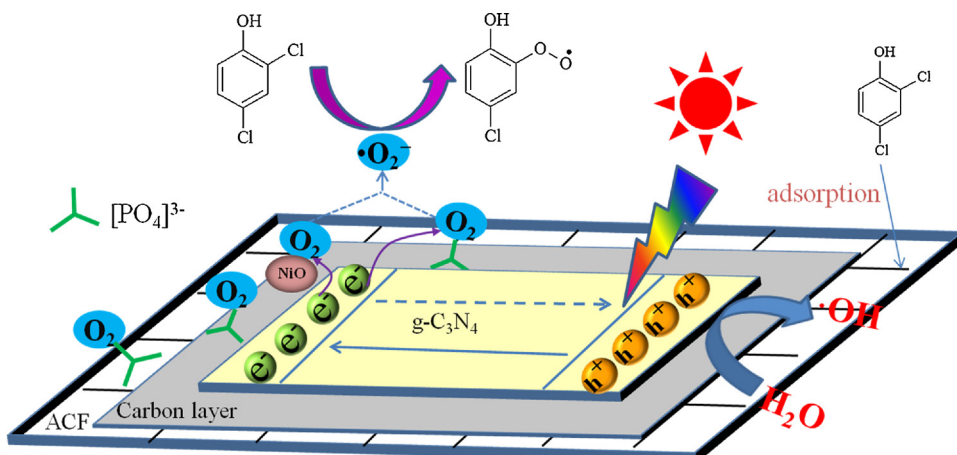


**Fig. 7.** Schematic of transfer and separation of photogenerated charges, along with their initial photochemical reactions on phosphoric acid-modified CN/nickel-regulated carbon layer-ACF.

enhanced charge separation and hence obtain high photocatalytic activities. Moreover, it is demonstrated that  $\cdot\text{O}_2^-$  is the dominant active species for 2,4-DCP degradation with a possible decomposition pathway based on the radical-trapping experiments and detected main intermediates. The present study is believed to be significant to design and prepare recyclable and highly efficient  $\text{g-C}_3\text{N}_4$ -based supported photocatalysts for purifying environmental contaminants.

## Acknowledgements

We are grateful for financial support from the NSFC project (U1401245, 21501052 and 91622119), the Program for Innovative Research Team in Chinese Universities (IRT1237), the Project of Chinese Ministry of Education (213011A), the Scientific Research Foundation for the Returned Overseas Chinese Scholars of Heilongjiang Province (LC2016003), and the Science Foundation for Excellent Youth of Harbin City of China (2014RFYXJ002).

## Appendix A. Supplementary data

Supplementary material related to this article can be found, in the online version, at doi:<https://doi.org/10.1016/j.apcatb.2018.10.008>.

## References

- Q.L. Ma, Y.F. Yu, M. Sindoro, A.G. Fane, R. Wang, H. Zhang, *Adv. Mater.* 29 (2017) 1605361–1605379.
- M.A. Shannon, P.W. Bohn, M. Elimelech, J.G. Georgiadis, B.J. Marinas, A.M. Mayes, *Nature* 452 (2008) 301–310.
- E.O. Scott-Emuakpor, A. Kruth, M.J. Todd, A. Raab, G.I. Paton, D.E. Macphee, *Appl. Catal. B Environ.* 123 (2012) 433–439.
- E. Pulido-Melián, O. González-Díaz, J.M. Doña-Rodríguez, J. Araña, J. Pérez-Peña, *Appl. Catal. A Gen.* 455 (2013) 227–233.
- M. Pera-Titus, V. García-Molina, M.A. Bano, J. Giménez, S. Esplugas, *Appl. Catal. B Environ.* 47 (2004) 219–256.
- S. Chiron, C. Minero, D. Vione, *Environ. Sci. Technol.* 41 (2007) 3127–3133.
- J. Xu, Z. Cao, X. Liu, H. Zhao, X. Xiao, J.P. Wu, X.H. Xu, J.L. Zhou, *J. Hazard. Mater.* 317 (2016) 656–666.
- Z.P. Cao, M.H. Zhang, J.L. Zhang, H.W. Zhang, *Bioresour. Technol.* 212 (2016) 138–143.
- P.Y. Dong, G.H. Hou, X.G. Xi, R. Shao, F. Dong, *Environ. Sci. Nano* 4 (2017) 539–557.
- E.B. Simsek, *Appl. Catal. B Environ.* 200 (2017) 309–322.
- G.S. Liu, S.J. You, H. Huang, M. Ma, N.Q. Ren, *Chemosphere* 171 (2016) 702–709.
- J. Tian, Y.H. Leng, Z.H. Zhao, Y. Xia, Y.H. Sang, P. Hao, J. Zhan, M.C. Li, H. Liu, *Nano Energy* 11 (2015) 419–427.
- S.N. Haberreutinger, L. Schmidt-Mende, J.K. Stolarczyk, *Angew. Chem. Int. Ed.* 52 (2013) 7372–7408.
- T. Yui, A. Kan, C. Saitoh, K. Koike, T. Ibusuki, O. Ishitani, *ACS Appl. Mater. Interfaces* 3 (2011) 2594–2600.
- M.M. Khin, A.S. Nair, V.J. Babu, R. Murugana, S. Ramakrishna, *Energy Environ. Sci.* 5 (2012) 8075–8109.
- Y. Bi, M.F. Ehsan, Y. Huang, J. Jin, T. He, *J. CO<sub>2</sub> Util.* 12 (2015) 43–48.
- C. Wang, O. Ranasingha, S. Natesakhawat, P.R. Ohodnicki Jr., M. Andio, J.P. Lewis, C. Matranga, *Nanoscale* 5 (2013) 6968–6974.
- C. Tang, L.F. Liu, Y.L. Li, Z.F. Bian, *Appl. Catal. B Environ.* 201 (2017) 41–47.
- Z.F. Bian, J. Zhu, H.X. Li, J. Photochem. Photobiol. C 28 (2016) 72–86.
- Y. Wang, X. Zhao, Y. Tian, Y.B. Wang, A.K. Jan, Y.T. Chen, *Chem. Eur. J.* 23 (2017) 419–426.
- Z.X. Pei, J.X. Gu, Y.K. Wang, Z.J. Tang, Z.X. Liu, Y. Huang, J.X. Zhao, Z.F. Chen, C.Y. Zhi, *ACS Nano* 11 (2017) 6004–6014.
- H.L. Tian, H.Q. Fan, J.W. Ma, Z.Y. Liu, L.T. Ma, S.H. Lei, J.W. Fang, C.B. Long, *J. Hazard. Mater.* 341 (2018) 102–111.
- X.C. Wang, K. Maeda, A. Thomas, K. Takanabe, G. Xin, J.M. Carlsson, K. Domen, M. Antonietti, *Nature Mater.* 8 (2009) 76–80.
- S.C. Yan, Z.S. Li, Z.G. Zou, *Langmuir* 25 (2009) 10397–10401.
- G. Liu, P. Niu, C.H. Sun, S.C. Smith, Z.G. Chen, Gao Qing (Max) Lu, H.M. Cheng, *J. Am. Chem. Soc.* 132 (2010) 11642–11648.
- J.Q. Tian, Q. Liu, A.M. Asiri, A.O. Al-Youbi, X.P. Sun, *Anal. Chem.* 85 (2013) 5595–5599.
- L.W. Zhang, Y.J. Wang, H.Y. Cheng, W.Q. Yao, Y.F. Zhu, *Adv. Mater.* 21 (2009) 1286–1290.
- L. Pellegrino, N. Manca, T. Kanki, H. Tanaka, M. Biasotti, E. Bellingeri, A.S. Siri, D. Marre, *Adv. Mater.* 24 (2012) 2929–2934.
- X.C. Yan, Y. Jia, J. Chen, Z.H. Zhu, X.D. Yao, *Adv. Mater.* 28 (2016) 8771–8778.
- C. Wang, W. Wan, Y.H. Huang, J.T. Chen, H.H. Zhou, X.X. Zhang, *Nanoscale* 6 (2014) 5351–5358.
- J.A. Rodri'guez-Manzo, C. Pham-Huu, F. Banhart, *ACS Nano* 5 (2011) 1529–1534.
- Marta Sevilla, Antonio B. Fuertes, *Carbon* 44 (2006) 468–474.
- M.J. Xie, J. Yang, J.Y. Liang, X.F. Guo, W.P. Ding, *Carbon* 77 (2014) 215–225.
- L.Q. Jing, J. Zhou, J.R. Durrant, J.W. Tang, D.N. Liu, H.G. Fu, *Energy Environ. Sci.* 5 (2012) 6552–6558.
- Y. Cao, L.Q. Jing, X. Shi, Y.B. Luan, J.R. Durrant, J.W. Tang, H.G. Fu, *Phys. Chem. Chem. Phys.* 14 (2012) 8530–8536.
- C. Liu, L.Q. Jing, L.M. He, Y.B. Luan, C.M. Li, *Chem. Commun.* 50 (2014) 1999–2001.
- J. Xu, L.W. Zhang, R. Shi, Y.F. Zhu, *J. Mater. Chem. A* 1 (2013) 14766–14772.
- J. Mao, T.Y. Peng, X.H. Zhang, K. Li, L.Q. Ye, L. Zan, *Catal. Sci. Technol.* 3 (2013) 1253–1260.
- F. Wang, P. Chen, Y. Feng, Z. Xie, Y. Liu, Y. Su, Q. Zhang, Y. Wang, K. Yao, W. Lv, G. Liu, *Appl. Catal. B Environ.* 207 (2017) 103–113.
- G.M. Zhou, D.W. Wang, L.C. Yin, N. Li, F. Li, H.H. Cheng, *ACS Nano* 6 (2012) 3214–3223.
- D. Deng, J.Y. Lee, *Chem. Mater.* 20 (2008) 3360–3367.
- Q.L. Li, Y.H. Zhang, G.X. Chen, J.Q. Fan, H.Q. Lan, Y.Q. Yang, *J. Catal.* 273 (2010) 167–176.
- F.X. Ma, J. Wang, F.B. Wang, X.H. Xia, *Chem. Commun.* 51 (2015) 1198–1201.
- J. Jiang, K. Zhao, X.Y. Xiao, L.Z. Zhang, *J. Am. Chem. Soc.* 134 (2012) 4473–4476.
- H.J. Wang, F. Raziq, Y. Qu, C.L. Qin, J.S. Wang, L.Q. Jing, *RSC Adv.* 5 (2015) 85061–85064.
- Z.Y. Sun, H.Q. Yuan, Z.M. Liu, B.X. Han, X.R. Zhang, *Adv. Mater.* 17 (2005) 2993–2997.
- Z.S. Wu, W.C. Ren, L. Wen, L.B. Gao, J.P. Zhao, Z.P. Chen, G.M. Zhou, F. Li, H.M. Cheng, *ACS. Nano* 6 (2010) 3187–3194.
- Z.S. Li, S.Y. Yang, J.M. Zhou, D.H. Li, X.F. Zhou, C.Y. Ge, Y.P. Fang, *Chem. Eng. J.* 241 (2014) 344–351.
- L. Korosi, I. Dekany, *Colloid Surf. A Physicochem. Eng. Asp.* 280 (2006) 146–154.
- L. Zou, H. Wang, X. Wang, *ACS Sustainable Chem. Eng.* 5 (2017) 303–309.
- H.Y. Zhou, Q. Sun, X. Wang, L.L. Wang, J. Chen, J.D. Zhang, X.H. Lu, *Sep. Purif. Technol.* 132 (2014) 346–353.
- Y.D. Liu, N. Sun, S.Y. Chen, R. Yan, P. Li, Y. Qu, Y.C. Qu, *Nano Res.* 11 (2018) 1612–1624.